

---

## Predicting CO<sub>2</sub> and CH<sub>4</sub> Transport in Landfill Gas Using Porous Inorganic Membranes Operated in The Darcy Regime

Edward Gobina<sup>\*1</sup>, Priscilla Ogunlode<sup>1</sup>, Ofasa Abunumah<sup>1</sup>, Ayo Giwa<sup>2</sup>,  
Firdaus Muhammad-Sukki<sup>3</sup>

---

<sup>\*</sup>e.gobina@rgu.ac.uk, ORCID: 0000-0003-0769-9427

<sup>1</sup>School of Engineering, Robert Gordon University, Aberdeen, United Kingdom

<sup>2</sup>McAlpha, Inc., 205 - 279 Midpark Way SE, Calgary, AB, Canada T2X 1M2

<sup>3</sup>School of Engineering, Edinburgh Napier University, Edinburgh, United Kingdom

**Abstract** The present work is focusing on the utilization of previously fabricated membrane to study the effect of pressure drop and temperature on permeability. Mass transfer considerations were used under previously optimized conditions. Subsequently, gas permeation study was conducted on ceramic membranes in CO<sub>2</sub> and small molecules present in biogas and it was found that the permeance of CO<sub>2</sub> and CH<sub>4</sub> decreased in the order of 15 nm > 200 nm > 6,000 nm, according to the decrease in pore size of the membranes. The transport of pure gases through a microporous composite membrane is also discussed. The membrane consists of an alumina support with mean pore diameters of 15, 200 and 6,000 nm and a TiO<sub>2</sub> washcoat top (separation) layer. The theory of Knudsen diffusion, laminar flow and Darcy flow are used to describe the transport mechanisms. It appears for the composite membrane that Knudsen diffusion occurs in the top layer and combined Knudsen diffusion/laminar flow in the support at pressure levels at 60 kPa and below. As pore sizes reduce further, and finally disappear, the transport process that takes over in a non-porous membrane is solution-diffusion—is a far simpler process than the complex, surface-mediated adsorption-surface diffusion occurring in the finest-scale porous membranes. For all experiments described below, the gauge pressure was kept lower than these critical pressures.

**Keywords:** Membrane, Pore size, nanoporous, Permeance, Biogas, Mechanism

### INTRODUCTION

THE use of ceramic membranes for various applications in industry has been gaining interest. These membranes are used as a support for separation and reaction processes that require high pressure drops, variable pH and temperatures even above 1000°C. Due to their versatility, they can be combined with other materials to form composites that are tailored to certain reactions such as desalination of water, hydrogenation, oxidation, CO<sub>2</sub> reforming, hydrogen separation and hydrogen peroxide synthesis [1-4].

Therefore, they may be made up of the support layer which is usually macro-porous and provides mechanical support; one or two intermediate layers that may be mesoporous linking the pore size differences between the layers and a top layer that is microporous and acts as the reaction site [5]. Ceramic membranes are typically made from one or a combination of metal oxides such as alumina (Al<sub>2</sub>O<sub>3</sub>), silica (SiO<sub>2</sub>), zirconia (ZrO<sub>2</sub>), titania (TiO<sub>2</sub>) depending on the

specific process requirement. They may also be in plate, disc or tubular form; however, the tubular form is typically used as it offers more separation area per unit volume for reaction to take place.

Some types of inorganic membranes include ceramic membranes formed by combining a metal and non-metal oxide, nitride or carbide; glass membranes which are made by leaching on de-mixed glasses; and metallic membranes obtained by sintering of metal powders. These membranes may be porous or non-porous. Porous membranes contain fixed pores, and their selectivity is dependent on the pore size but their physical and chemical properties which interpret the permeability depend on the material used and method of preparation. On the other hand, the non-porous membrane depends on the intrinsic properties of the material. Porous membranes are characterized by pore size, porosity, and tortuosity. Pore sizes range from microporous ( $d_p < 2\text{nm}$ ), mesoporous ( $2\text{nm} < d_p < 50\text{nm}$ ) and macroporous ( $d_p > 50\text{nm}$ ) [6].



**Figure 1.** Ceramic Membranes [7]

Membranes usually need supports and these can be prepared by several methods to give the desired characteristics. These include sintering, extrusion, track etching, acid leaching and sol gel [8]. Over the last few decades, much research has been done on the CO<sub>2</sub> separation especially in biogas upgrading to biomethane [9]. The presence of CO<sub>2</sub> in the biogas reduces the calorific value of the raw gas methane recovery during the combustion and other downstream processes [10]. Similarly, the presence of CO<sub>2</sub> decreases the heating value of natural gas and causes equipment corrosion in the existence of water [11]. Meanwhile, membrane separation technology has received much attention in CO<sub>2</sub> separation mainly due to its advantages compared to the conventional separation technologies [12]. Inorganic membranes are generally favored in the CO<sub>2</sub> separation among the membrane materials over polymeric membranes due to their specific unique characteristics, including well-specified pores, the molecular filtering property, ability to sustain longevity and wide pore size availability [13,14].

Ceramic membranes are highly permeable membrane materials that show chemical stability against CO<sub>2</sub> and other landfill gas components. This project addresses the materials stability challenge by developing highly stable eco-friendly ceramic microporous membranes that can lead to a proof-of-concept (PoC) module for integrated CO<sub>2</sub> capture in landfill using the setup shown in Figure 1. Experiments are conducted to demonstrate a link between porosity and pores size on membrane permeance. This will enable the future investigation of four possible loadings

of affinity material on the membrane and up to two flow designs using computational fluid dynamics (CFD), finite element method stress analysis (FESA) and incorporating various transport mechanisms. After evaluating the advantages and disadvantages of each pore size and porosity, we have selected the 200 nm as the most promising one. The new designs will comprise up to two asymmetric membranes on opposite side of an interlayer that provide both mechanical stability and flow channels for the biogas. The components will be configured in a tubular metal housing forming the permeator. With our collaborators, we will also identify and produce a wide range of materials at the lab scale for high throughput and stability. The applications of these type of membranes are wide in range and the team will in the future focus the membrane technology demonstration on a microporous CO<sub>2</sub> transport mechanisms including surface flow that has superior performance regarding high CO<sub>2</sub> permeability, infinite methane selectivity, and high thermal, chemical, and mechanical stability. Furthermore, our intention is in the development of additional optimized membranes using both standard Al<sub>2</sub>O<sub>3</sub> and multiple phase membranes. Highly stable materials that will be identified by project partners will also be considered for use with technologies like integrated catalytic membrane reactors for producing chemical energy carriers such as ammonia, hydrogen and other aspects of the developing energy transition leading to net-zero. In addition to CO<sub>2</sub>-capture and methane upgrading, this technology can be applied to the field of CO<sub>2</sub>-utilisation, waste destruction or pure gas separation. The deliverables of this project will benefit members of the scientific community working on gas separation membranes and other industries in the circular economy where carbon capture is important such as fossil power exhaust gas, fossil fuel upgrading in refinery flue gas and in iron and steel plants. It will also benefit the wider public through climate change mitigation.

## **EXPERIMENTAL**

The ceramic membranes have been used as received without any further modifications and typically made of aluminum oxide, titanium oxide, and zirconium oxide which all belong to the group of inorganic materials and are stable under CO<sub>2</sub> and water vapour conditions of biogas. The center of the illustration below shows the membrane experimental set up rig (Fig 2) and membrane holder with seal in place (Fig 3a) and without seal in place (Figure 3b) The pressure is set with a test gas, where a continuous flow over the sample is ensured using a pressure regulator (PR), and the pressure is maintained by a pressure controller (PC). The pressure and temperature are measured using a pressure indicator (PI) and temperature indicator (TI) respectively.

## **MATERIALS AND METHODS**

### **Scanning Electron Microscopy (Zeiss EVO LS-10) and Energy Dispersive X-ray Detector (Oxford Instruments, INCAX-act 51-ADD0020)**

Samples were prepared by freezing in liquid nitrogen and then fracturing to prevent deformation of the membrane structure and analysis was done in the order magnitude of 2000x and the difference in surface morphology is very clear with more defects shown in the 6000nm sample compared with the less defective surface of the 15nm and 200nm membranes. EDXA/FTIR/Physisorption for all membranes samples are alike containing the same compounds and prepared similarly.

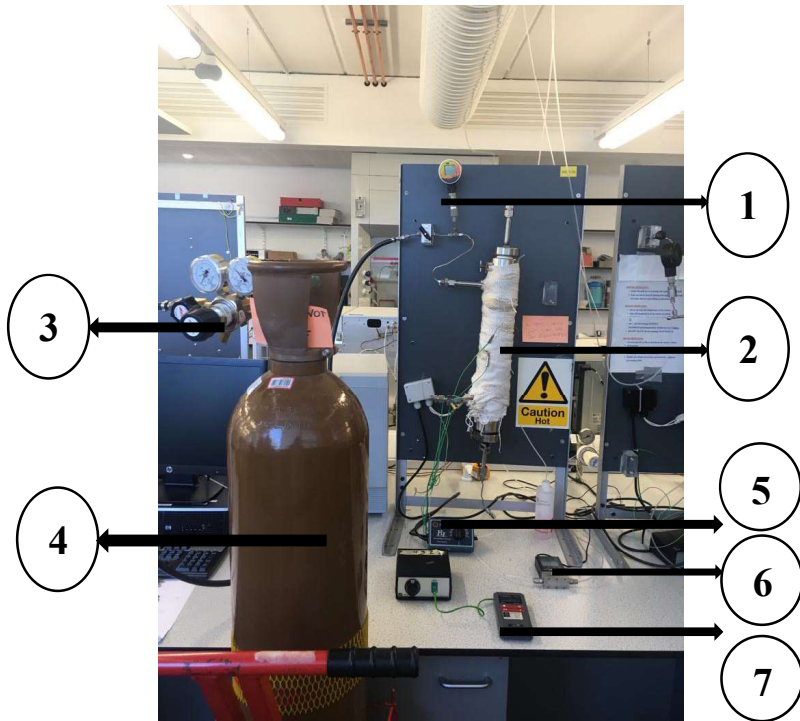


**Figure 2** Experimental set-up; pressure gauge(1), membrane module covered with heating tape(2), gas regulator(3), gas cylinder(4), heat regulator(5), volumetric meter(6) and temperature indicator(7)



**Figure 3a** Membrane core holder with seal



**Figure 3b** Membrane core holder without seal

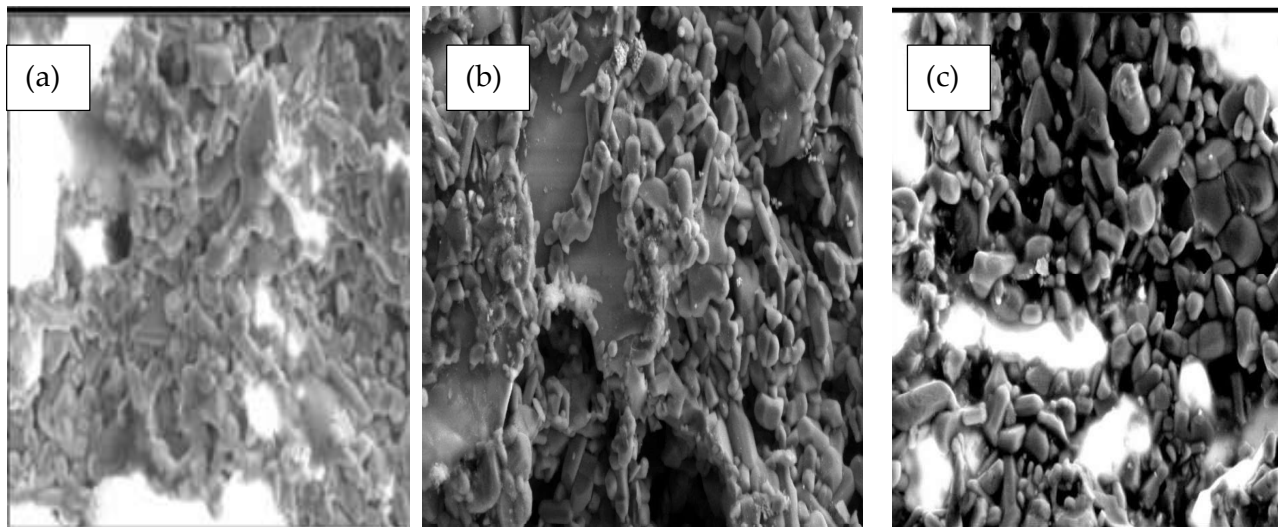


**Figure 4** Outer surface SEM micrograph of (a) 15 nm membrane (b) 200 nm membrane (c) 6000 nm membrane.

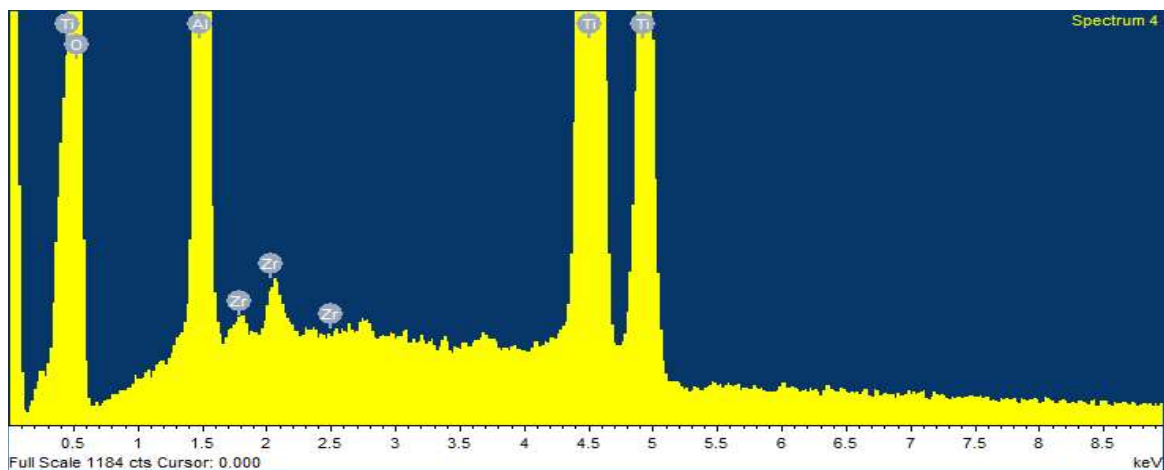


Figure 5. EDXA for 6,000nm membrane

### Fourier-Transform Infrared Spectroscopy (FT-IR)

FTIR is used to obtain an infrared spectrum of absorption or emission of a solid, liquid or gas. The spectrometer concurrently stores high-resolution spectral data over a wide spectral range. Peaks show a reduction in this transmittance and means that the infrared light of a certain wave number is being absorbed by the functional group within the membrane sample and therefore not reaching the detector to give information on the type of bond within that compound.

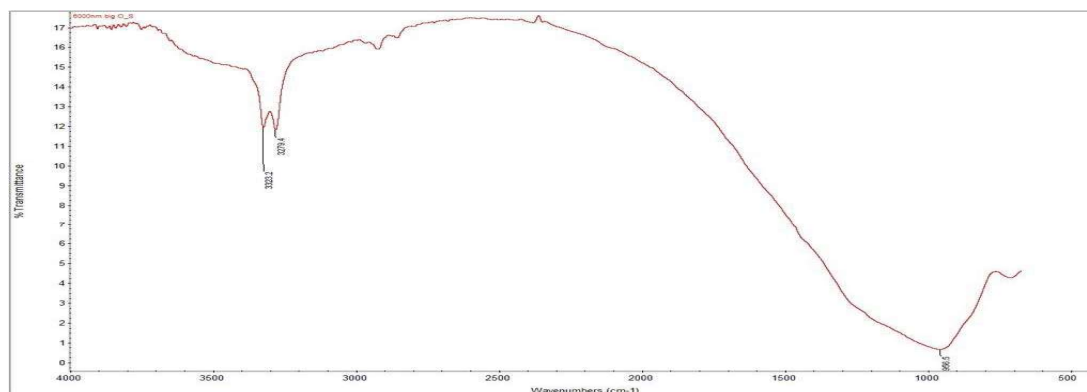
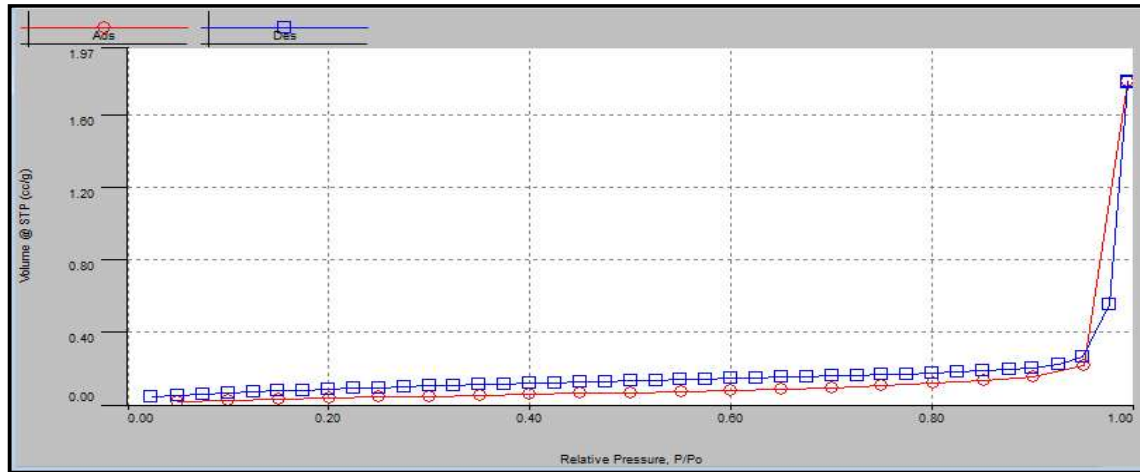


Figure 6. 6000nm outer surface

### Liquid Nitrogen Adsorption

The N<sub>2</sub> adsorption/desorption isotherms are of type IV; they are presented as a hysteresis loop which is typical for mesoporous material. Nitrogen adsorption at 77 K is a standard and widely used technique for the determination of pore size distribution, specific surface area and pore volume for meso and microporous membranes. The adsorption isotherm which is the quantity of gas (vapour) adsorbed on a solid at various pressures, at constant temperatures, is a function of the pore size and surface area of the solid and hence can provide important information about the two parameters. The BET surface area is one of the physical

characteristics of membranes which determine how much gas can be adsorbed or accommodated per gram of the material. Higher surface area is preferred since it is an indication of the greater amount of gas that can be adsorbed on the pore surface of the membrane. Porous inorganic membranes are commonly characterized in terms of their pore size and pore size distribution. In comparing the pore size of the membrane to the size of the gas molecules and keeping the other parameter constant, the gas permeability across the membrane to some extent follows the sequence of diameter of the gas molecules in a decreasing order.



**Figure 7** N<sub>2</sub> Adsorption/Desorption Isotherms of the 6000nm Membrane

### **Gas Permeation Tests**

Permeation experiments and stability tests were conducted for CH<sub>4</sub> and CO<sub>2</sub> using the flow rig shown in Figure 2. These membranes are to be scaled up for the prototype-module for use as the reference base materials. The membrane components were sealed in the proof-of-concept (PoC)-module and tested under realistic operating conditions of 20 – 100°C and pressure drops of 1 – 3 bars. Initially, the membrane sample was degassed by holding both upstream and downstream under vacuum with a series of valves closed and to select a small downstream volume or opened to select a large volume. The system leak rate was determined by manipulating a particular valve for at least 1 hour and measuring the rate of downstream pressure rise.

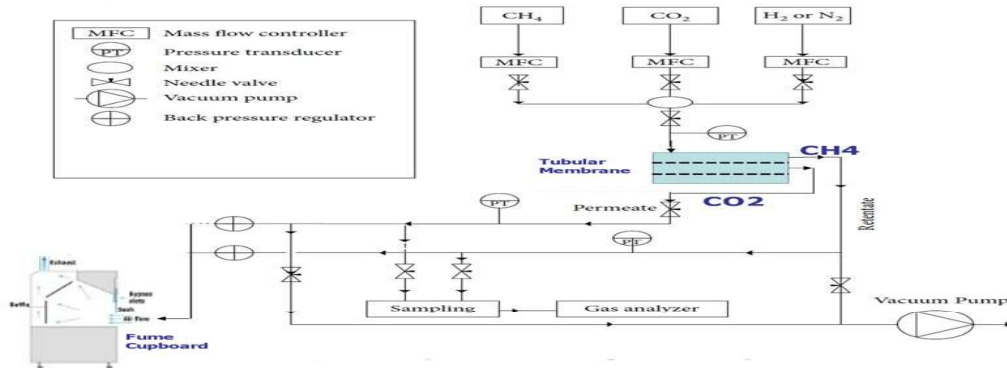


Figure 8 Schematic of the Laboratory Gas Permeation Set Up

## RESULTS AND DISCUSSIONS

### Parallel Transport Through Membranes

In order to experimentally demonstrate these mechanisms, three separate membranes with three pore sizes were investigated in this work (15nm, 200nm and 6000nm). If we ignore the surface flow, molecular sieving and capillary condensation contributions as these will be negligible in this pore size range equation reduces to:

$$P_T = P_{H-P} + P_{Kn} \quad (1)$$

Which can be written in full as follows:

$$P_T = [(\phi/\tau)(P/8\mu RT)r_p^2] + [(4/3)(\sqrt{2/\pi})(\phi/\tau)(1/\sqrt{RTM_a})r_p] \quad (2)$$

where:

$$P_{H-P} = [(\phi/\tau)(P/8\mu RT)r_p^2] \quad (3)$$

$$P_{Kn} = [(4/3)(\sqrt{2/\pi})(\phi/\tau)(1/\sqrt{RTM_a})r_p] \quad (4)$$

In equations 1-4,

$P_T$  is the total permeability ( $\text{mol m m}^{-2} \text{s}^{-1} \text{Pa}^{-1}$ )

$\phi$  is porosity of the membrane (-)

$\tau$  is the pore tortuosity (-)

$M_a$  is the molecular mass ( $\text{kg/kmol}$ )

$R$  is the gas constant ( $8.31446 \text{ J mol}^{-1} \text{ K}^{-1}$ )

$T$  is the absolute temperature (K)

$P$  is the transmembrane pressure (Pa)

$\mu$  is the gas viscosity ( $\text{Pa s}^{-1}$ )

$r_p$  is the membrane pore radius (m)

### 4.2 Parameter Estimation for Theoretical Calculation of Permeance

Figure 9 describes these three distinct transport mechanisms acting individually or simultaneously. (A) Bulk diffusion. (B) Knudsen diffusion. (C) Surface diffusion.

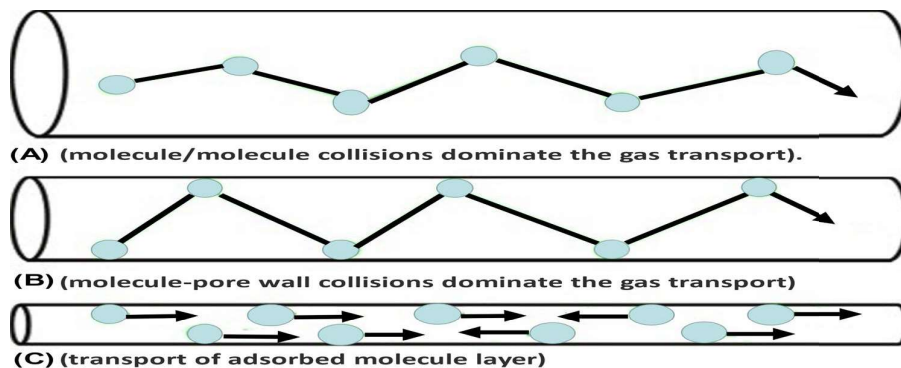


**Figure 9:** Three distinct mechanisms acting individually or simultaneously. (A) Bulk diffusion (B) Knudsen diffusion. (C) Surface diffusion

The limiting values of the pore size regarding the diffusion types can be estimated as:

- If  $r_p < 1 \times 10^{-7}$  m, Knudsen diffusion dominates.
- If  $r_p > 1 \times 10^{-7}$  m, bulk diffusion dominates.
- If  $1 \times 10^{-7}$  m  $< r_p < 1 \times 10^{-5}$  m, both Knudsen and bulk diffusion can exist.
- If  $2 \times 10^{-9}$  m  $< r_p < 50 \times 10^{-9}$  m, surface diffusion can exist.

### Hagen-Poiseuille

Molecule/molecule collisions dominate the gas transport.

**Table 1** H-P Parameters

$P_{H-P} = [(\phi/\tau)(P/8\mu RT)]r_p^2$	gamma-Al <sub>2</sub> O <sub>3</sub>
$P$ (Pa-1)	101.0
$T$ (K)	293 393
$R$ (J K <sup>-1</sup> mol <sup>-1</sup> )	8.31
$r_p$ (nm)	15, 200, 6000
$\mu$ (Pa-s)	Viscosity of methane at 20°C = $1.10 \times 10^{-5}$ Viscosity of methane at 100°C = $1.35 \times 10 \times 10^{-5}$ Viscosity of CO <sub>2</sub> at 20°C = $1.47 \times 10 \times 10^{-5}$ Viscosity of CO <sub>2</sub> at 100°C = $1.85 \times 10 \times 10^{-5}$
$\phi/\tau$ (Dimensionless)	0.0375 for 15nm pore size,  0.0619 for 200nm pore size and  0.016 for 6000nm pore size

### Knudsen Diffusion

Molecule-pore wall collisions dominate the gas transport.

**Table 2** Knudsen Parameters

$P_{Kn} = [(4/3)(\sqrt{2/\pi})(\phi/\tau)(1/\sqrt{RTM_a})r_p]$	gamma-Al <sub>2</sub> O <sub>3</sub>
$\phi/\tau$ (Dimensionless)	0.0375 for 15nm pore size,  0.0619 for 200nm pore size and  0.016 for 6000nm pore size
$T$ (K)	293 393
$M_a$ (kg/kmol)	CO <sub>2</sub> = 44 CH <sub>4</sub> = 16
$R$ (J K <sup>-1</sup> mol <sup>-1</sup> )	8.31 J mol <sup>-1</sup> K <sup>-1</sup>

**Table 3** Calculated Permeability

Membrane Pore Size	Temperature	$P_{TCH_4}$ (Calculated)	$P_{TCO_2}$ (Calculated)
nm	(°C)	(mol m m <sup>-2</sup> s <sup>-1</sup> Pa <sup>-1</sup> )	(mol m m <sup>-2</sup> s <sup>-1</sup> Pa <sup>-1</sup> )
15	20	4.46E-12	3.12E-12
	100	3.23E-12	2.19E-12
200	20	8.39E-10	6.23E-10
	100	1.82E-09	1.32E-09
6000	20	1.34E-07	1.00E-07
	100	8.57E-08	6.25E-08

### Measured Permeance

The experimental permeance and theoretical permeance calculated by the equation 2 are shown in Table 4 below (for two temperatures 20 °C and 100 °C respectively and for each pore size) using the parameters presented in Tables 2 and 3 and using consistent units of mol m m<sup>-2</sup> s<sup>-1</sup> Pa<sup>-1</sup>.

**Table 4** Measured Permeance

Membrane Pore Size	Temperature	$P_{TCH_4}$ (Calculated)	$P_{TCO_2}$ (Calculated)
nm	(°C)	(mol m m <sup>-2</sup> s <sup>-1</sup> Pa <sup>-1</sup> )	(mol m m <sup>-2</sup> s <sup>-1</sup> Pa <sup>-1</sup> )
15	20	4.46E-06	3.12E-06
	100	3.23E-06	2.19E-06
200	20	8.39E-07	6.23E-07
	100	1.82E-06	1.32E-06
6000	20	1.34E-04	1.00E-04
	100	8.57E-05	6.25E-05

### Comparison of the Experimental Permeance and Theoretical Permeance

Convective flow occurs through large pores (> 10,000nm or > 1000 Å) and separation does not take place. Knudsen diffusion takes place through pores (1,000–10,000nm or 100–1000 Å) –

where pores having diameter less than the mean-free path ( $\lambda$ ) of the gas molecules will allow the lighter molecules to preferentially diffuse through the pores. Molecular sieving or surface diffusion occurs in pores in the range (50–1,000nm or 5 - 100 Å) – here large molecules are excluded from the pores based on their size. We can denote  $F_T$  as the total permeance which is simply the permeability/membrane thickness ( $P_T/\delta$ ), ( $\text{mol m}^{-2} \text{s}^{-1} \text{Pa}^{-1}$ ). Under the mesoporous condition ( $2\text{nm} < d_p < 50\text{nm}$ ) Knudsen diffusion can occur. Permeability of  $\text{CH}_4$  and  $\text{CO}_2$  by Knudsen diffusion can be easily estimated based on the inverse of the square root of molecular weight relationship with flux and because it is difficult to know the exact thickness of the membrane in the case of microporous membrane, the value of gas permeation is usually expressed by the unit of permeance ( $\text{mol m}^{-2} \text{s}^{-1} \text{Pa}^{-1}$ ; where permeance = permeability/thickness of membrane). The values of permeance were on the order between  $10^{-4}$  and  $10^{-7}$ . Because the thickness of such membrane is usually micron–submicron size, the permeability will be less than  $10^{-8} \text{ mol m}^{-2} \text{ s}^{-1} \text{ Pa}^{-1}$ . So, for the 15 nm membrane a thickness of the order of  $10^{-6}$  m has been estimated, for the 200nm membrane we estimate a thickness of  $10^{-3}$  m while a thickness of  $10^{-3}$  m has been estimated for the 6000nm membrane as confirmed by scanning electron microscopy [16]. If we now use these estimated membrane thicknesses, we can convert the permeabilities in Table 3 to permeance units  $\text{mol m}^{-2} \text{s}^{-1} \text{Pa}^{-1}$ . As can be seen from the Table 5, the experimental gas permeance in 15 nm pore membrane have excellent agreement with the measured gas permeance for both temperatures and gases. With the increase of the pore size, there is a slight discrepancy between the experimental gas permeance and theoretical gas permeance. The experimental gas permeance through the nanopores is generally higher than that predicted by the parallel flow equation by one order of magnitude (or two), and the H-P equation considerably underestimates gas flux in the nanoscale pores.

**Table 5:** Comparison of Measured and Calculated Permeance

Membrane Pore Size	Temperature	$F_{T\text{CH}_4}$ (Measured)	$F_{T\text{CH}_4}$ (Calculated)	$F_{T\text{CO}_2}$ (Measured)	$F_{T\text{CO}_2}$ (Calculated)
nm	(°C)	( $\text{mol m}^{-2} \text{s}^{-1} \text{Pa}^{-1}$ )			
15	20	3.4187E-06	4.46E-06	2.2137E-06	3.12E-06
	100	3.4381E-06	3.23E-06	2.1999E-06	2.19E-06
200	20	3.0379E-06	8.39E-07	2.0221E-06	6.23E-07
	100	3.0379E-06	1.82E-06	2.0387E-06	1.32E-06
6000	20	1.3526E-06	1.34E-04	8.7283E-07	1.00E-04
	100	1.357E-06	8.57E-05	8.7283E-07	6.25E-05

The outputs predicted by the transport mechanistic model are compared to the actual experimental measurements tabulated in Table 5 and a parity plot is used to display the quality of the fit. The figures show the mechanistic model predicted results obtained by applying the transport model and the experimentally measured values. The value of the global error obtained by the minimization process is of 11.2 % for  $\text{CO}_2$  and of 2.7 % for  $\text{CH}_4$ . The results demonstrate that the parallel transport model is accurate in predicting the experimental results in the range of the explored working conditions, especially as regards the lower pores size range.

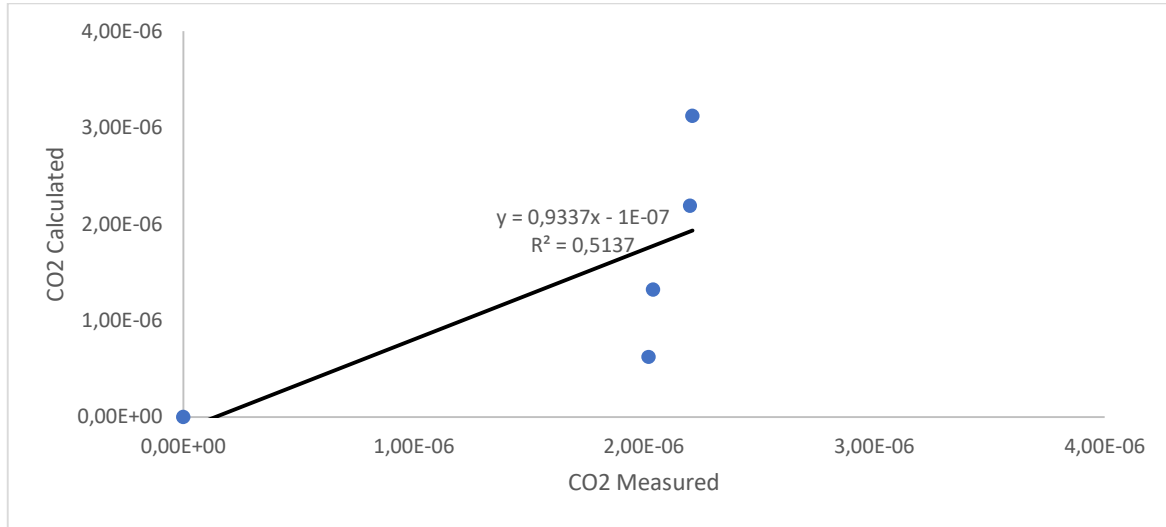


**Figure 10** Parity Diagram to Compare Mechanistic Model Prediction and Measured Permeance

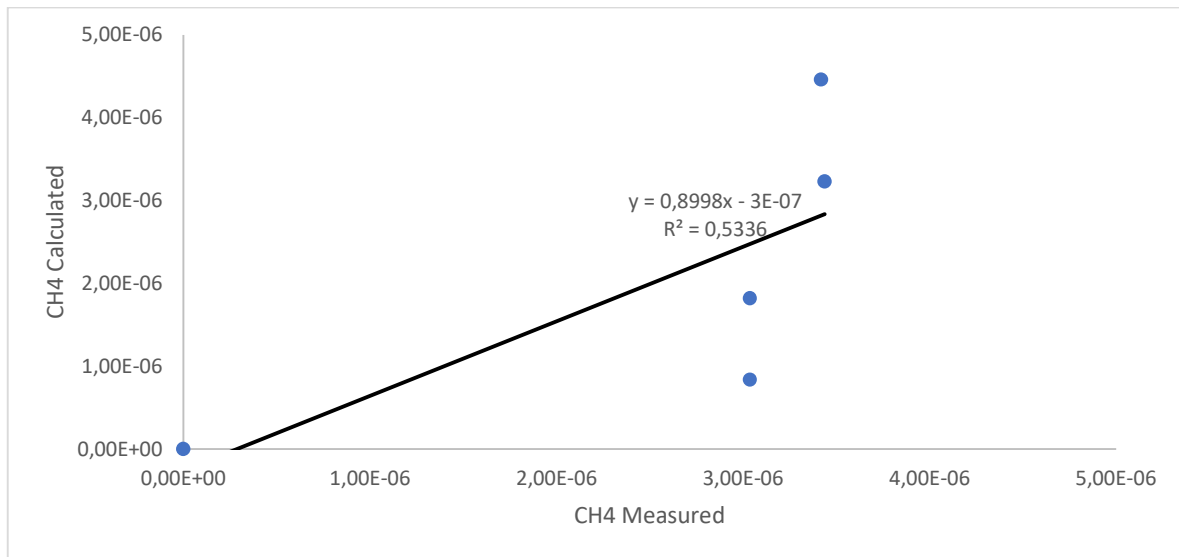


**Figure 11** Parity Diagram to Compare Mechanistic Model Prediction and Measured Permeance

### Membrane Selectivity

The results for the gas permeation experiment with the three membranes summarized in Table 6 in terms of the gas permselectivity. These are compared with the ratio of the square root of the inverse of the molecular weights and the ratio of the viscosities. It is observed that the measured permselectivities are extremely close to the ideal Knudsen values while calculated permselectivities are extremely close to the ideal viscous flow values. Based on Knudsen flow, separation factors for several gas pairs have been calculated and they represent ideal separation factors. For Knudsen flow, the selectivity ratio or the separation factor for gases can be

estimated from the square root of the ratio of the molecular weights. In viscous flow regime, the distance between gas molecules is smaller compared to the transverse channel. Subsequently, the main driving force in viscous flow mechanism is molecule to molecule collisions, minimal interaction with the pore walls, high permeability and little or no separation is achieved since the viscosities of gases are awfully close to each other i.e.,  $r_p > \lambda$ . In terms of temperature, the results show an overall increase in CH<sub>4</sub> flowrate as temperature increases from 20°C to 100°C. CO<sub>2</sub> collides with the pore walls more than CH<sub>4</sub> and loses momentum and absolute velocity to the wall with each temperature increase. An increase in temperature has thus no improvement in the membrane selectivity as seen in the Table 6 below where the selectivity at 100°C is remarkably similar to selectivity at 20°C. This is explained by ratio of methane to carbon dioxide increasing with the rise in temperature showing that the interaction of the gases with the membrane begin to change taking the experimental selectivity values closer to the ideal selectivity.

**Table 6:** Comparison of Measured and Calculated Permselectivity, Ideal Knudsen and Ideal Viscous Flow

Membrane Pore Size (nm)	Temperature (°C)	$F_{T\text{CO}_2}/F_{T\text{CH}_4}$ (Measured Permselectivity)	$F_{T\text{CO}_2}/F_{T\text{CH}_4}$ (Calculated Permselectivity)	$\sqrt{MW_{\text{CH}_4}}/\sqrt{MW_{\text{CO}_2}}$ Ideal Knudsen selectivity	$\mu_{\text{CH}_4}/\mu_{\text{CO}_2}$ Ideal Viscous Flow selectivity
15	20	0.65	0.70	0.60	0.75
	100	0.64	0.68	0.60	0.73
200	20	0.67	0.74	0.60	0.75
	100	0.67	0.73	0.60	0.73
6000	20	0.65	0.75	0.60	0.75
	100	0.64	0.73	0.60	0.73

The correlation of calculated permeance ratio and measured permeance ratio, ideal Knudsen selectivity and ideal viscous flow selectivity is presented in figure 10 and 11 and the correlation coefficient of calculated permeance ratio and measured permeance ratio is  $y=1.102x - 0.0002$  with the correlation coefficient ( $R^2$ ) of 0.9953. The results of these correlation analyses indicate a significant correlation of measured permeance ratio and calculated permeance ratio.

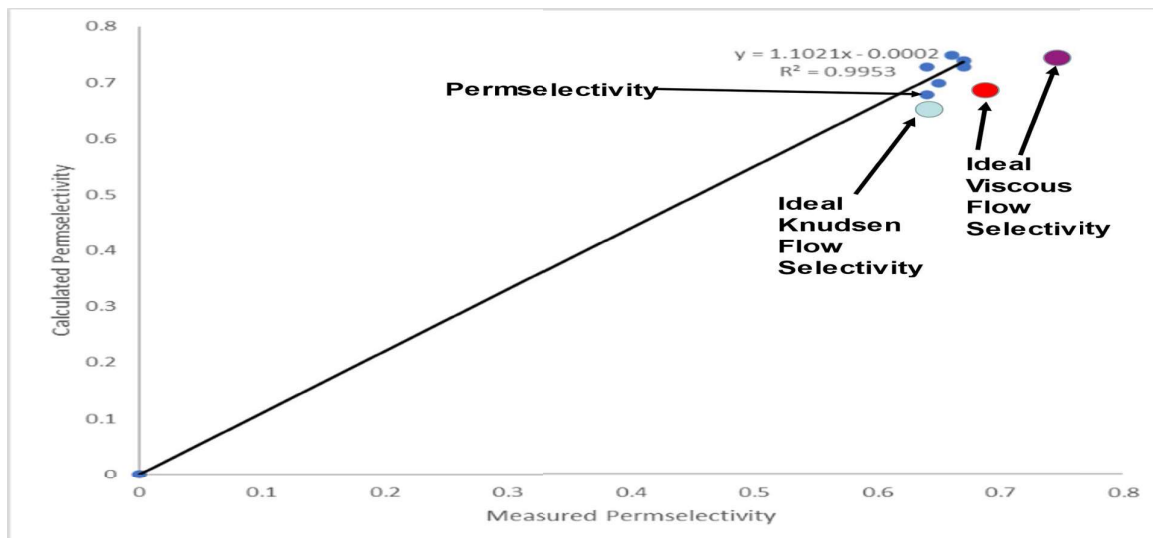


Figure 12 Parity Diagram to Compare Mechanistic Selectivity Model and Measured Selectivity

### Effect Of Membrane Pore Size on Permeance

It was confirmed that lower pore sizes improved the separation performance of the membrane. The 15 nm membrane offered greater permeance when compared with membranes of higher pore size as shown in the following figures 13 and 14. Nonetheless, with regards to preferential gas flow, methane had a higher flux than carbon dioxide, this was not to be expected as the kinetic diameter of CO<sub>2</sub> is less than that on CH<sub>4</sub>. This means that molecular sieving (or size exclusion) is not the prevalent flow mechanism at play within the pressure and temperature ranges used. In this case, Knudsen diffusion is prevalent following the relation between fluid flow and molecular weight as deduced from Graham's law of diffusion. Furthermore, a quadratic curve is noticed in the figures which is in the form  $y=a+bx+cx^2$  and can be linked to the parallel flow model described by De Meis et al [15], which confirms the interplay of viscous and Knudsen diffusion within these membranes. It appears that Knudsen diffusion occurs on the top membrane layer (having a lower average/mean pore size) while a combination of laminar flow and Knudsen diffusion takes place in other layers. Thus, for effective separation, we require the introduction of a dominant flow mechanism such as surface diffusion to cause significant interaction of the target gas molecules with the pore surfaces (16).

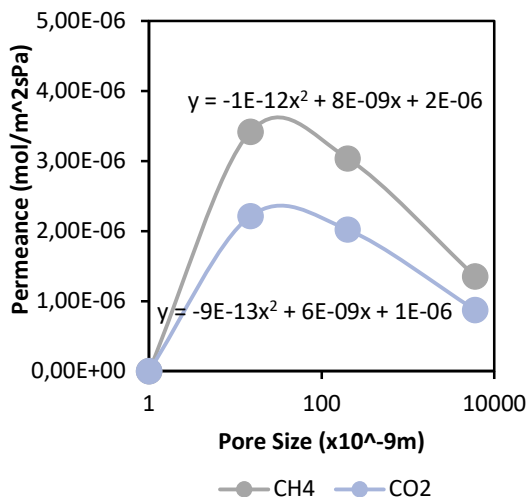


Figure 13. Effect of membrane pore size on gas permeance at 3 bar and 20°C

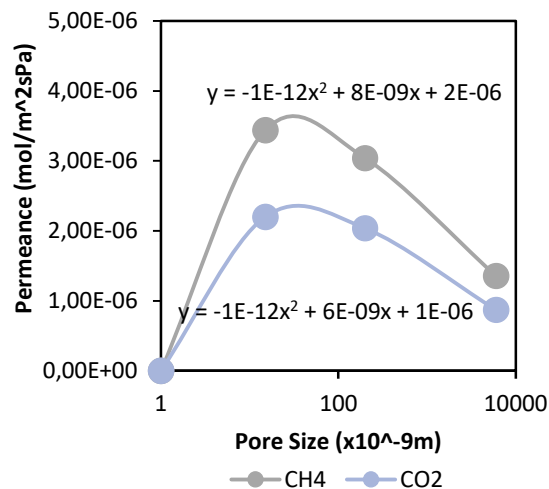


Figure 14. Effect of membrane pore size on gas permeance at 3 bar and 100°C

## CONCLUSION

This study has confirmed that under all situations of temperature and pressure drops investigated in this study the mass transfer rate from the bulk gas stream to the membrane surface was significantly greater than the permeation rate. This confirms that mass transfer conditions are not limiting. Membranes with 15 - 6000 nm pore sizes are difficult to implement in gas separation. The ceramic membranes in this study show ideal selectivity almost identical to the Knudsen value and lower than the ratio of viscosities (viscous flow) though better selectivity will be achieved with decreasing pore size below 15 nm. However, this study therefore confirms that Knudsen diffusion can occur in the microporous range due to more molecule/pore wall collision depending on the type of gases used. In this case, the membrane selectivity values were in the ideal Knudsen selectivity range for CO<sub>2</sub> and CH<sub>4</sub> gases due to the differences in the molecular weight of the gases. The presence of viscous flow limits the separation properties being initiated by Knudsen diffusion. Thus, for effective separation, we require the introduction of a dominant flow mechanism such as surface diffusion to cause significant interaction of the target gas molecules with the pore surfaces and further improve the membrane performance. The results show the difference in surface morphology is very clear with 139 more defects shown in the 6000 nm sample compared with the more closely-knit 140 structures of the 15 nm and 200nm samples. Unlike CH<sub>4</sub>, CO<sub>2</sub> shows a higher adsorption on many metal oxide surfaces at the pressures and temperatures and this property will be investigated in further work to increase the selectivity of CO<sub>2</sub> and therefore the purity of CH<sub>4</sub>.

## REFERENCES

- [1] Hsieh HP. Inorganic membranes for separation and reaction. Elsevier; 1996 Jun 7.
- [2] Fain DE. Mixed gas separation technology using inorganic membranes. *Membrane Technology*. 2000 Apr 1;2000(120) pp9-13.
- [3] Kanellopoulos NK, 2000. Recent advances in gas separation by microporous ceramic membranes.
- [4] Oyama ST, Yamada M, Sugawara T, Takagaki A, Kikuchi R. Review on mechanisms of gas permeation through inorganic membranes. *Journal of the Japan Petroleum Institute*. 2011;54(5) pp298-309.
- [5] Li K. Ceramic membranes for separation and reaction. John Wiley & Sons; 2007 Apr 30.
- [6] Ghasemzadeh K, Basile A, Iulianelli A. Progress in modeling of silica-based membranes and membrane reactors for hydrogen production and purification. *ChemEngineering*. 2019 Mar;3(1):2.
- [7] Guochu Technology [Internet].; 2016 Available from: Available from: <http://www.guochukeji.com/en/bzsb/moyuanjian/4312.html?msclkid=a646d4439c5b14910b6fb5d2af8ebb8f>
- [8] Tasselli F. Membrane Preparation Techniques. In: Drioli E, Giorno L, editors. *Encyclopedia of Membranes* [Internet]. Berlin, Heidelberg: Springer Berlin Heidelberg; 2015 pp1–3. Available from: [https://doi.org/10.1007/978-3-642-40872-4\\_1825-1](https://doi.org/10.1007/978-3-642-40872-4_1825-1)
- [9] Angelidaki, et al., Biogas upgrading and utilization: current status and perspectives, *Biotechnol. Adv.* 36(2) (2018), pp452-466
- [10] I.U. Khan, et al., Biogas as a renewable energy fuel – a review of biogas upgrading, utilisation and storage, Volume 150, 15 October 2017, pp277-294
- [11] M. RAL MAMUN AND S. TORII (2019) Sustainable energy & fuels 3 (1), pp166-172
- [12] A.G. Chmielewski, A. Urbaniak, K. Wawryniuk, Membrane enrichment of biogas from two-stage pilot plant using agricultural waste as a substrate, *Biomass Bioenergy*, 58 (2013), pp219-228
- [13] S.O. Masebinu, A.O. Aboyade, E. Muzenda, Parametric study of single and double stage membrane configuration in methane enrichment process, *World Congr. Eng. Comput. Sci.*, 2 (2014), pp1-9
- [14] S.Z.A.Seman (2019) Optimizing purity and recovery of biogas methane enrichment process in a closed landfill *Renewable Energy*, Volume 131, pp1117-1127
- [15] De Meis, D. Gas-transport-through-porous-membranes. *ENEA* 2017, pp1-19.
- [16] Ngozi Claribelle Nwogu, Mohammed Kajama and EdwardGobina (2015) A study of gas diffusion characteristics on a micro porous composite silica ceramic membrane, Volume 134, 15 December 2015, pp 1044-1050.